Carbon Resources Conversion 5 (2022) 15–25

Contents lists available at ScienceDirect

Carbon Resources Conversion

journal homepage: www.keaipublishing.com/en/journals/carbon-resources-conversion

Insights on copper, manganese, and Nickel/ZSM-5 catalytic mechanisms for nitric oxides selective reduction with ammonia

Cheng Liu [a,c], Running Kang [a,b,d], Feng Bin [a,b,*], Xiaolin Wei [a,b], Kwun Nam Hui [e], Saravanan Kasipandi [d], Kwan San Hui [f,**]

[a] State Key Laboratory of High-Temperature Gas Dynamics, Institute of Mechanics, Chinese Academy of Sciences, Beijing 100190, PR China
[b] School of Engineering Science, University of Chinese Academy of Sciences, Beijing 100049, PR China
[c] School of Automobile Engineering, Wuhan University of Technology, Wuhan 430070, PR China
[d] Department of Chemical and Metallurgical Engineering, School of Chemical Engineering, Aalto University, Kemistintie 1 P.O. Box 16100, Espoo FI-00076, Finland
[e] Institute of Applied Physics and Materials Engineering, University of Macau, Avenida da Universidade, Taipa, Macau, PR China
[f] School of Engineering, Faculty of Science, University of East Anglia, Norwich Research Park NR4 7TJ, United Kingdom

ARTICLE INFO

Keywords:
Selective catalytic reduction
Transition metals
ZSM-5
Reaction mechanism
Kinetics

ABSTRACT

The elucidation of the selective catalytic reduction mechanisms over state-of-the-art metal-promoted zeolites is essential for nitric oxides removal in automobile and stationary source applications. In this work, H/ZSM-5 catalysts modified with transition metals, including copper, manganese, and nickel, were prepared by using an incipient wetness impregnation method and were evaluated for the selective reduction of nitric oxides with ammonia. Results indicate that copper/ZSM-5 exhibits the highest catalytic activity, with > 90% nitric oxide conversion at a broad operation temperature window (221–445 °C). The nitric oxide conversion profiles of nickel/ZSM-5 shows two peaks that correspond to weak activity among the catalysts; the low-temperature peak (290 °C) was induced by nickel clusters dispersed on the ZSM-5 surface, while the high-temperature peak (460 °C) was assigned to the bulk nickel oxides. The size of granular nickel monoxide crystallites with an exposed (2 0 2) plane is 2–30 nm, as confirmed by Scanning electron microscopy, X-ray diffraction, and Transmission electron microscope measurements. Temperature-programmed reductions with hydrogen results testified that the copper and nickel cations, as the main species contributing to selective catalytic reduction, were reduced via $Cu^{2+}/Cu^{+}\rightarrow Cu^{0}$ and $Ni^{2+}\rightarrow Ni^{0}$ for copper/ZSM-5 and nickel/ZSM-5, respectively, while for the manganese/ZSM-5, the Mn^{3+} species in manganese clusters were reduced to Mn^{2+} by hydrogen. Particularly, temperature-programmed desorption coupled with mass spectrometer (TPD-MS) and in situ diffuse reflectance infrared Fourier transform spectroscopy (DRIFTS) were comprehensively used to reveal the relationship between zeolite structure and catalysts' properties for improving selective catalytic reduction. These results confirm that the ammonia is adsorbed and activated on both Brønsted and Lewis acid sites. The nitrous oxide desorbs in two stages during nitric oxide-TPD-MS measurements, corresponding to the desorption of nitric oxide bounded to amorphous clusters and the nitric oxide strongly bounded to bulk metal oxides, respectively. The selective catalytic reduction process follows the L-H mechanism at low temperatures, in which nitric oxide and ammonia molecules were adsorbed and activated on the catalyst surface. The selective catalytic reduction rates reached the maximum value of 1.8×10^{8} (218 °C), 6.4×10^{7} (227 °C), and 3.9×10^{7} s^{-1} (235 °C) for copper, manganese, and nickel /ZSM-5, respectively.

1. Introduction

Nitric oxides ($NO_x = NO + NO_2$) emissions from the combustion of fossil fuels remain a major source of air pollution in automobile and stationary source applications, which are the major cause of acid rain, smog, and ozone depletion [1]. Complying with the latest regulated

* Corresponding author at: State Key Laboratory of High-Temperature Gas Dynamics, Institute of Mechanics, Chinese Academy of Sciences, Beijing 100190, PR China.
** Corresponding author.
E-mail addresses: binfeng@imech.ac.cn (F. Bin), k.hui@uea.ac.uk (K.S. Hui).

https://doi.org/10.1016/j.crcon.2021.11.002
Received 30 June 2021; Received in revised form 6 October 2021; Accepted 15 November 2021
Available online 20 November 2021

standards merely by improving the combustion technology is no longer possible; thus, selective catalytic reduction of nitric oxides with ammonia (NH_3-SCR) has been successfully demonstrated at the commercial scale and currently represents the most effective NO_x abatement technology [2-5]. In recent years, the elucidation of the SCR catalytic mechanisms over state-of-the-art metal-promoted zeolites has been investigated as a key topic [6-11]. The ZSM-5 zeolite is porous crystalline aluminosilicates of natural or synthetic origin with a three-dimensional, open-anion framework consisting of oxygen-sharing SiO_4 and AlO_4 tetrahedra. When transition metals are introduced via ion exchange process, the prevailing opinion seems to be that different species are present on the ZSM-5 support: (i) metal cations located in the zeolite channels, (ii) dispersed oxide clusters, and (iii) bulk particles arising from metal silicate for metal over-exchanged ZSM-5 samples [12-15]. These species that are formed may arise partially from an appropriate amount of acid sites and the threshold effect of ZSM-5 channels, which is beneficial to dispersing the metal ions and preventing the aggregation of metal species to form relevant oxides. However, a comprehensive and satisfactory account is still lacking, particularly for what concerns the standard SCR reaction ($NO + O_2 + NH_3$) [16]. With the increase in reaction temperature, dispersed clusters and bulk particles are widely accepted to be active in turn over M/ZSM-5 (M = ferrum, copper, manganese, cobalt, nickel, cerium, and Lanthanum, etc.) catalysts, where general factors related to active windows, such as ion exchange ratio, dispersion of metal oxide, and metal valence state, are generalized systematically from different studies. The isolated metal cations play only an indirect role, allowing chemisorption of nitric oxide (NO) in the form of nitrosyls and acting as storage sites. According to Bellmann et al. [17], however, the larger oxide/silicate species are mainly involved in unselective parallel combustion reactions. An often encountered problem is that nitric oxides conversion profiles possess double peaks [18], that is, a low-temperature peak (LT-peak) and a high-temperature peak (HT-peak). The identification of the LT-peak has been the subject of some debate. Sullivan et al. [19] and Kieger et al. [20] assigned it to a transient peak considering the temperature-programmed reaction condition, whereas Li et al. [21] attributed it to a permanent peak. The Co/ZSM-5 catalyst in our previous study confirmed that the LT-peak in the nitric oxides conversion profile was considered a permanent peak [22]. The LT-peak (<300 °C) is induced by cobalt ions and the amorphous cobalt oxide clusters, while the HT-peak (>300 °C) is assigned to the crystalline cobalt oxides. When the cobalt loading ratio increases, the overlapping LT- and HT-peaks contribute to SCR active windows (NO_x conversion > 95%). On the whole, the SCR mechanism over two issues is not sufficiently understood and remains the subject of in-depth investigation.

The reaction mechanisms for NH_3-SCR over ZSM-5-based catalysts, including details such as active sites and reaction pathways, also remain a topic of debate. Concerning the reaction pathway over catalysts, many researchers suggested that NH_3 is adsorbed and activated on the Brønsted and/or Lewis acid centers to form intermediates (NH_4^+ or $–NH_2$), which then react with gaseous nitric oxide to decompose into N_2 and H_2O through the Eley–Rideal mechanism [23-25]. Another is the Langmuir-Hinshelwood (L-H) mechanism, in which the adsorbed nitric oxides could react with the NH_3/NH_4^+ species adsorbed on acid sites to form different intermediates and then produce N_2 and H_2O. [26,27]. Kijlstra et al. [28] investigated the $NO + O_2$ co-adsorption behaviors by using Fourier transform infrared spectroscopy (FTIR) and summarized the thermal stabilities of absorbed species following the order nitrosyl < monodentate nitrites < bridged nitrates < bidentate nitrates. Here, the main methods applied for the estimation and characterization of nitric oxide and ammonia adsorption sites (the latter also corresponds to acidic sites) on the catalyst surface is TPD in a carrier gas flow [29]. The kinetic process of adsorbed ammonia and nitric oxide on active sites is still unclear ascribe to the lack of necessary qualitative and quantitative analysis of adsorbed species.

To further study the NH_3-SCR of nitric oxides, the fundamental mechanism information was provided and discussed to correctly relate the observed catalytic activity of the Cu/ZSM-5, Mn/ZSM-5, and Ni/ZSM-5 catalysts. In terms of qualitative means, diffuse reflectance infrared Fourier transform spectroscopy (DRIFTS) was employed to investigate the adsorption characteristics of nitric oxides species and as the interaction of ammonia with Brønsted and Lewis acid sites. The reactions between gaseous ammonia or ($NO + O_2$) with adsorbed nitric oxides or ammonia were explored by transient DRIFTS. Therefore, the surface intermediates produced under reaction conditions ($NO + NH_3 + O_2$) were also investigated. In terms of quantitative means, the TPD of nitric oxide and ammonia is combined with MS technique (NO- and NH_3-TPD-MS), which is conducted to ascertain the correlation between strength and stability of intermediates and the activity during the nitric oxide and ammonia adsorption/desorption on the catalyst surface. On this basis, a kinetic model was established to study the changes of NO/NH_3 coverage and reaction rate related to the increase in bed temperature over catalysts. The obtained detailed reaction pathway will provide information to understand the role of metal doping zeolite catalysts in SCR reaction, which is facilitate in designing a better catalytic system to remove nitric oxides in automobile and stationary source applications.

2. Experimental

2.1. Catalyst preparation

H/ZSM-5 with an atomic Si/Al ratio of 25 and crystallinity of 100% was supplied by Nankai University, Tianjin, P.R. China. The M/ZSM-5 (M = Cu, Mn, and Ni) catalysts were prepared by using an incipient wetness impregnation method with an appropriate amount of nitrates, corresponding to 0.05 mole copper, manganese, and nickel, respectively, dissolved in deionized water and mixed with 50 g H/ZSM-5. The resulting solution was stirred at 80 °C for 24 h at a pH of about 7.0. After being dried by evaporation, the sample was calcined in air at 600 °C for 4 h. The copper, manganese, and nickel contents of calcined catalysts were determined by inductively coupled plasma atomic emission spectrometer (ICP-AES) analysis, shown in Table S1. Prior to each catalytic activity testing, the catalyst was pressed into a given tool at a pressure of 10 MPa and then granulated and screened to a size of 20–40 meshes.

2.2. Characterization

Scanning electron microscopy (SEM) images and semi-quantitative analyses of micron-sized spots were conducted by using a Hitachi S-4800 field emission scanning electron microscope, in combination with an EDAX Genesis 4000 energy-dispersive X-ray spectrometer (EDX). Specimens for SEM investigation were fixed on aluminum holders by using adhesive conductive graphite tape. The crystalline phase of each sample was determined by powder X-ray diffraction (XRD) using a Rigaku D/MAC/max 2500v/pc diffractometer with Cu Kα radiation (40 kV, 200 mA, λ = 1.5418 Å). Transmission electron microscope (TEM) images of catalysts were observed with a Philips Tecnai G^2 F20 microscope operating at 200 kV coupled with an Oxford-1NCA EDX detector. Prior to TEM analysis, samples were dispersed in ethanol by sonication and deposited on a copper grid coated with a carbon film. X-ray photoelectron spectroscopy (XPS) was performed with a Kratos Axis Ultra DLD spectrometer using Mg Kα radiation. The binding energies were referenced to the C 1 s line at 284.8 eV from adventitious carbon. Temperature-programmed reductions with hydrogen (H_2-TPR) experiments were performed with a TP5080B chemisorption analyzer, coupled with a thermal conductivity detector (TCD). Then, 100 mg of the sample was pretreated in 20% oxygen at 600 °C for 30 min. After cooling to 50 °C, the H_2-TPR was recorded in 10% H_2/He, with a heating rate of 10 °C/min and a final temperature of 800 °C. Temperature-programmed desorption of oxygen, NO, and NH_3 (O_2-, NO- and NH_3-TPD) was conducted in a TP5080B chemisorption analyzer, monitored by a TCD and

an online quadrupole mass spectrometer (MS, Pfeiffer PrismaPlus). After being pretreated at 300 °C under flowing helium (50 ml/min) for 1 h, the powder sample (100 mg) was cooled to 50 °C and then adsorbed to saturation by 5% O_2/He, 5% NO/He, or 5% NH_3/He for 0.5 h. Physically adsorbed O_2, NO or NH_3 on the catalyst was removed by flushing the sample with helium (50 ml/min) for 1 h at the adsorption temperature. Thermal desorption signals were recorded in the temperature range of 50–1000 °C at an increasing temperature rate of 10 °C/min. In situ infrared spectroscopy was recorded on a Bruker Tensor 27 spectrometer equipped with a mercury cadmium telluride detector. Prior to each IR spectra, the sample was pretreated in N_2 flow at 400 °C to remove adsorbed impurities.

2.3. Catalytic activity testing

Catalytic experiments were performed at atmospheric pressure in a flow-type apparatus designed for continuous operation. A total of 0.5 g of the catalyst was packed into a fixed-bed reactor made of a quartz tube with an internal diameter of 4 mm. A K-type thermocouple was placed inside the catalyst bed to monitor the reaction temperature. The reaction was carried out across the temperature range 50–500 °C, and the feed gas (450 ppm NO, 500 ppm NH_3, 5% O_2 and N_2 to balance; flow rate of 200 ml/min) was metered using calibrated electronic mass flow controllers. The effluent NO, NH_3, and O_2 were monitored by using a Maihak online multicomponent analyzer.

3. Results and discussion

3.1. Structure and morphology

Fig. 1 illustrates the SEM images of Cu/ZSM-5, Mn/ZSM-5, and Ni/ZSM-5 catalysts. The parent ZSM-5 is composed of irregularly localized, distinct-edged, and bright polycrystalline aggregates within the regular geometry. The ZSM-5 structure can be maintained after the addition of copper, manganese, and nickel, with a relatively average size of about 1 μm. Compared with the smooth and angular surface of Cu/ZSM-5 and Mn/ZSM-5, the surfaces of the ZSM-5 grains become much rougher and are coated with a layer of "star point" powders when the nickel is loaded, consisting of irregular nanosized species. The EDX/SEM result collected from a typical region (Point 1) gives a nickel composition of 3.44 at% for Ni/ZSM-5, which is higher than the chemical equivalence ratio, thus indicating that most of nickel species are enriched on the ZSM-5 surface.

The XRD patterns (Fig. 2) of H/ZSM-5 and catalysts doped with copper or manganese are characterized by peaks at 2θ = 7.9°, 8.8°, 23.1° and 23.8°, which represent the (0 1 1), (0 2 0), (0 5 1), and (0 3 3) planes

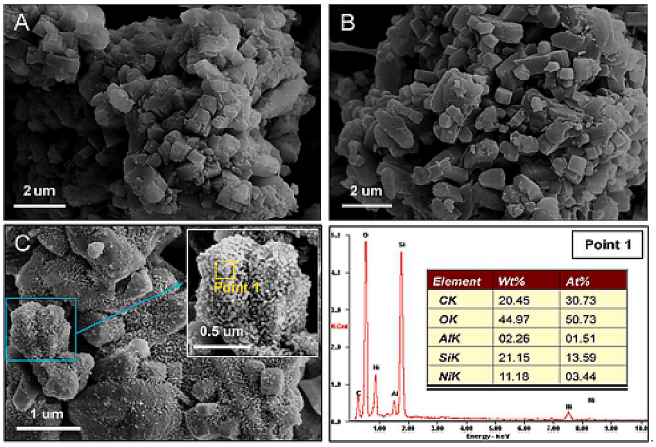

Fig. 1. SEM micrographs and EDX analysis for metal containing ZSM-5 catalysts: (A) Cu/ZSM-5, (B) Mn/ZSM-5 and (C) Ni/ZSM-5.

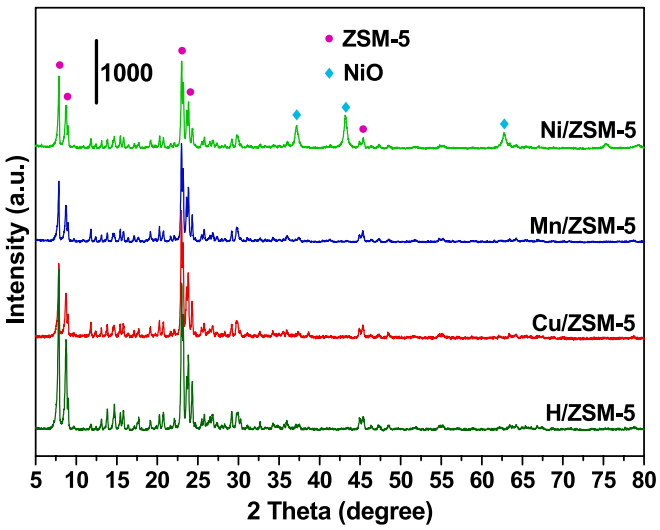

Fig. 2. Wide-angle XRD patterns of H/ZSM-5, Cu/ZSM-5, Mn/ZSM-5 and Ni/ZSM-5 catalysts after calcination in air at 600 °C for 4 h.

of their crystal structures, respectively. No diffraction peaks related to copper and manganese oxide crystals are detected, suggesting that these species are well dispersed on the ZSM-5 support. However, the nickel species are less dispersed on ZSM-5 with a larger crystallite size than copper and manganese, with the obtained diffractograms revealing the segregation of NiO (2θ = 37.2°, 43.3°, 62.9°, PDF 01-1239) over the Ni/ZSM-5 catalyst.

The TEM images (Fig. 3) display the ZSM-5 crystal structure with interference fringes. Some dark spots are apparent in Fig. 3A, which can be determined as amorphous copper oxides over Cu/ZSM-5. By contrast, the dispersed manganese oxides cannot be clearly observed (Fig. 3B) over the zeolite structure, but the expected manganese equivalence ratio over Mn/ZSM-5 is confirmed by ICP-AES analysis. Partial amorphous manganese oxides (marked as ellipses) are probably located on the outer surfaces of ZSM-5 crystals. Combined EDX/TEM analysis (Fig. 3C) supports heterogeneous nickel loading with detectable NiO crystallites

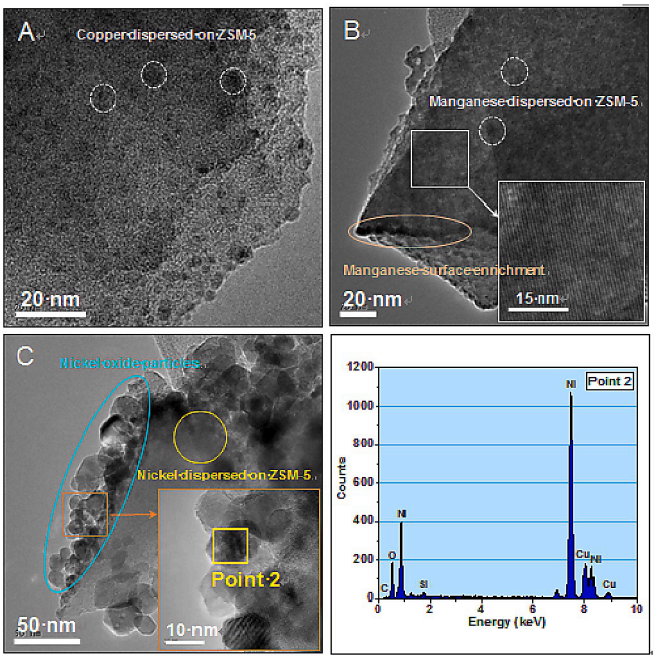

Fig. 3. TEM micrographs and EDX analysis for metal containing ZSM-5 catalysts: (A) Cu/ZSM-5, (B) Mn/ZSM-5 and (C) Ni/ZSM-5.

(Point 2) except for dispersed nickel oxides, which is in agreement with that of SEM. The NiO crystallites outside the pores of ZSM-5 have a granular form and a non-uniform size of 2–30 nm, with the lattice fringe of NiO particles (inset in Fig. 3C) being 0.208 nm, indicating that the supported NiO nanoparticles are exposed (2 0 2) plane.

3.2. XPS analysis of catalysts

XPS technology is used to obtain further information about the chemical state and composition of the elements on the surface of catalysts, which can show the potential active components that participate in SCR. Fig. 4A displays the main copper peaks containing two distinctive XPS peaks of Cu $2p_{3/2}$ and Cu $2p_{1/2}$ for Cu/ZSM-5, and both peaks centered at 933.6 ± 0.2 and 953.3 ± 0.2 eV are attributed to spin–orbit splitting of bivalent Cu^{2+} [30]. On the high binding energy side of the copper core line $2p_{3/2}$, the well-defined shake-up satellite peaks located at 942.0 and 944.3 eV are related to the multiple splitting in the $2p^5\ 3d^9$ final state, also as a fingerprint of Cu^{2+} species existing in Cu/ZSM-5. Curve fitting of the Cu$2p_{3/2}$ spectrum showed that a peak appeared at 933.8 eV along with a shoulder peak at 936.1 eV, where the former is assigned to Cu^{2+} in CuO and the latter to isolated Cu^{2+} and/or Cu^{2+} in $Cu(OH)_2$. Pure CuO and $Cu(OH)_2$ standards are analyzed and correspond to binding energies of 933.8 and 935.1 eV, respectively [31-33]. The relatively high binding energy of $Cu(OH)_2$ is characteristic of a charge transfer from the metal ion toward the support matrix [34]. Strong interaction between the metal ion and the support provides evidence that the ZSM-5 support promotes copper dispersion near the Brønsted and Lewis acid sites. For Mn/ZSM-5, the XP spectra of Mn 2p (Fig. 4B) exhibit two main peaks at 641.7 and 653.3 eV because of the $2p_{3/2}$ and $2p_{1/2}$ split spin orbit components of the manganese metal and can be interpreted as mainly arising from the Mn^{2+} oxidation state of MnO. Here, six fitting peaks of Mn $2p_{3/2}$ spectra are located at 640.2, 641.1, 642.1, 643.0, 644.2, and 645.2 eV with FWHM of about 1.70, in agreement with in previous literature [35]. Meanwhile, a magnitude of Mn 3 s peak splitting of ΔE = 5.5 eV, together with a shake-up satellite peak at about 647.0 eV, is also diagnostic of the oxidation state, with ΔE = 5.5 eV belonging to Mn^{2+} [36]. The XP spectrum of Ni/ZSM-5 (Fig. 4C) is typical of NiO with the main Ni $2p_{3/2}$ at 855.3 eV and a shake-up peak at about 862 eV [37]. Given the broadness of the peak, some contribution from $Ni(OH)_2$ is also expected. Hence, the experimental curve clearly contains two components: one typical of NiO oxide corresponding to the fitting peaks at 855.0, 856.4, and 861.4 eV, while the other up-energy shifted at 857.4 and 863.5 eV, which is indicative of $Ni(OH)_2$ [38]. The O 1 s XP spectra of Cu/ZSM-5, Mn/ZSM-5 and Ni/ZSM-5 catalysts are shown in Fig. 4D, where the band at a lower binding energy (530.1–530.8 eV) is related to the lattice oxygen from metal oxides, and another band at a higher binding energy (532.7 eV) corresponds to regular lattice oxygen from the ZSM-5 zeolite structure. For Mn/ZSM-5, the O 1 s XP spectra of manganese oxides is centered at 530.1 eV, which is within the range of 529.7 (Mn_2O_3) and 531.2 (MnO). In combination with the faint shake-up peak in Mn 2p spectra, we can conclude that the manganese oxides exist in the form of MnO and Mn_2O_3 over Mn/ZSM-5. Elemental compositions calculated from the areas of Si 2p, Cu 2p, Mn 2p, and Ni 2p peaks show that the surficial Cu/Si, Mn/Si, and Ni/Si atomic ratio for Cu/ZSM-5 (0.09), Mn/ZSM-5 (0.17), and Ni/ZSM-5 (0.19) are higher than those of the chemical equivalence ratio (0.06). The XPS results provide evidence that the surficial atomic ratio of nickel for Ni/ZSM-5 is approximately two times higher than that of copper for Cu/ZSM-5, indicating that part of Cu species is probably located in channel of ZSM-5 in the form of Cu ions. These results indicate that the copper, manganese, and nickel appear to become enriched on the surface of ZSM-5 grains.

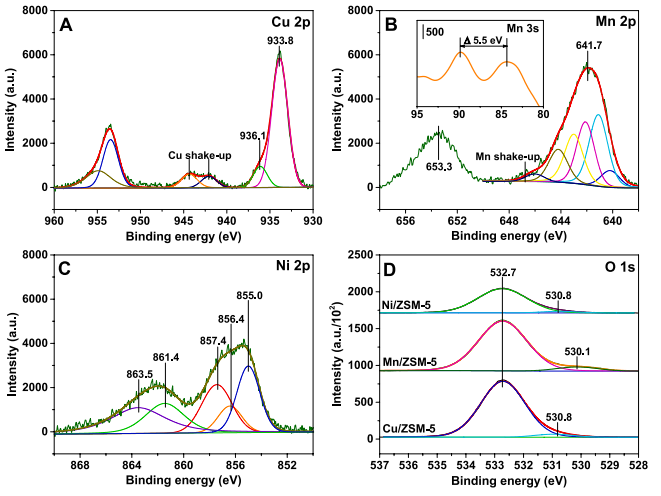

Fig. 4. XPS narrow spectra for Cu 2p (A), Mn 2p and Mn 3 s (B), Ni 2p (C), and O 1 s (D) for the Cu/ZSM-5, Mn/ZSM-5 and Ni/ZSM-5 catalysts.

3.3. Temperature-programmed analysis of the catalysts

H_2-TPR analysis is performed to investigate the reducibility of each catalyst, with the profiles presented in Fig. 5. The ZSM-5 support is almost unreducible under temperature conditions ranging from room temperature to 900 °C. Therefore, the reduction peaks here correspond to the reduction of different kinds of copper, manganese, and nickel oxides. The faint profile of Mn/ZSM-5 shows that only one reduction peak centered around 431 °C, which is generally assigned to the reduction of Mn_2O_3 that has been confirmed by XPS analysis. The Mn^{3+} species of manganese clusters is confirmed to only be reduced to Mn^{2+} by hydrogen at a temperature lower than 600 °C, proceeding via a one-step reduction with the stoichiometry of hydrogen [39]. However, pure MnO samples were prepared by reducing separately both Mn_2O_3 and the as-received MnO sample under a H_2 atmosphere at 1000 °C [40,41]. Two reduction peaks are found for Cu/ZSM-5: a sharp peak located at 289 °C is interpreted as the reduction of surficial CuO clusters on the external surface of the ZSM-5 framework, and another one—the peak (366 °C) in trace—is ascribed to the reduction of bulk CuO particles. Rabie et al. [42] testified that the XP spectrum of the reduced Cu/ZSM-5 showed only Cu $2p_{3/2}$ curve-fitted at 932.4 eV, assuming that the reduced catalyst was rich in Cu^0 species. Similar two reduction peaks are observed for Ni/ZSM-5, corresponding to the nickel clusters and bulk NiO reduced at 487 and 612 °C, respectively. The quantity of hydrogen

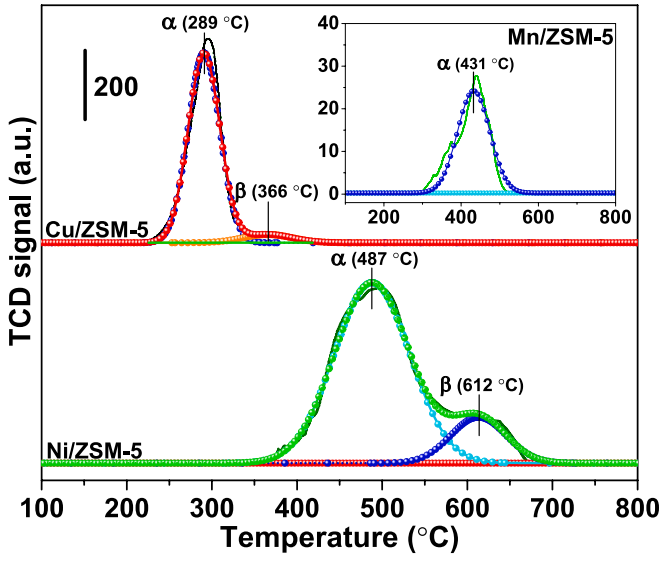

Fig. 5. H_2-TPR-TCD profiles of Cu/ZSM-5, Mn/ZSM-5 and Ni/ZSM-5 catalysts.

consumption is quantitatively analyzed and presented in Table 1, with the value decreasing in the order Ni/ZSM-5 (3.14 mmol/g) > Cu/ZSM-5 (1.49 mmol/g) > Mn/ZSM-5 (0.16 mmol/g). The XPS results provide evidence that the surficial atomic ratio of nickel for Ni/ZSM-5 is approximately two times higher than that of copper for Cu/ZSM-5, which corresponds to about two times higher hydrogen consumption for Ni/ZSM-5 than Cu/ZSM-5 here, considering that Cu^{2+} and Ni^{2+} reduced to Cu^0 and Ni^0, respectively, verified by the surficial atomic ratio of nickel for Ni/ZSM-5 is approximately two times higher than that of copper for Cu/ZSM-5 in the XPS results. Similarly, the Mn^{3+}/Mn^{2+} ratio can be determined as 0.12 based on the XPS results and the Mn^{3+} reduced to Mn^{2+}during H_2-TPR. Even so, the SCR catalytic activity test, which will be discussed in the subsequent section, confirms that the redox properties of catalysts decrease mainly according to their reduction temperature rather than hydrogen consumption, following the sequence of Cu/ZSM-5 > Mn/ZSM-5 > Ni/ZSM-5.

The O_2-TPD measurements are performed to investigate the mobility of oxygen species. On the basis of the results illustrated in Fig. 6, the pronounced desorption peaks obtained for all the catalysts can be classified into three parts. The asymmetric tailed peak, including α and β, is physically adsorbed oxygen in reversible molecular form because direct NH_3 desorption takes place as the temperature increases. Oxygen is also chemically adsorbed on amorphous metal oxides and/or surface oxygen vacancies on bulk metal oxides corresponding to the desorption at 415 °C for Cu/ZSM-5, 413 °C for Mn/ZSM-5, and 333 °C for Ni/ZSM-5 (γ peak). Here, a collective property of copper and zeolite leads to the formation of species containing extra-lattice oxygen, followed by metal cations that tend to increase their degree of oxidation to adsorb oxygen molecules or atoms with electrons [43]. The δ peak centered at the temperature > 700 °C is associated with the release of the bulk lattice oxygen bonded to matrix metal ions [44]. Quantitative results (Table 1) confirm that Cu/ZSM-5 obtains the most adsorbed oxygen desorption among all the catalysts. A considerable part of copper species enters the ZSM-5 channel, which is why the van der Waals force induced by exposing the micropores promotes the formation of physically adsorbed oxygen. The amount of chemisorption oxygen for Cu/ZSM-5, Mn/ZSM-5, and Ni/ZSM-5 are 0.06, 0.11, and 0.11 mmol/g, respectively, which are related to the metal surficial enrichment and beneficial to improving the oxygen mobility during SCR.

NH_3-TPD is measured and the profiles are shown in Fig. 7 to investigate the acid strength of catalysts and adsorbed ammonia that contribute to SCR reaction. For all the tested catalysts, the spectrum exhibits a main maximum at 100 °C. Thereafter, the rate of ammonia desorption decreases gradually, giving rise to a main shoulder with an unresolved maximum at about 380 °C. The broad desorption peak centered at about 100 °C is ascribed to weakly bound ammonia adsorbed physically on ZSM-5 or from nonzeolitic impurities (α + β peak, weak acid sites), because only the NH_3 signal (mass 17) is synchronously detected by the mass spectrometer (Fig. 8). The medium-temperature peak located within the range of 350–450 °C, such as 368 °C for Cu/ZSM-5 and 420 °C for Mn/ZSM-5, is attributable to ammonia bound to Brønsted acid sites (Si-OH and Al-OH) of ZSM-5 (γ peak, medium acid sites). No obvious medium acid sites are observed for Ni/ZSM-5 because of the enrichment of most nickel oxides. Our previous work confirmed that the Brønsted acid sites not only bind and disperse transition metal ions but also absorb and activate ammonia [45,46]. Hence, the role is contradictory because the metal ions dispersed here not only are unable

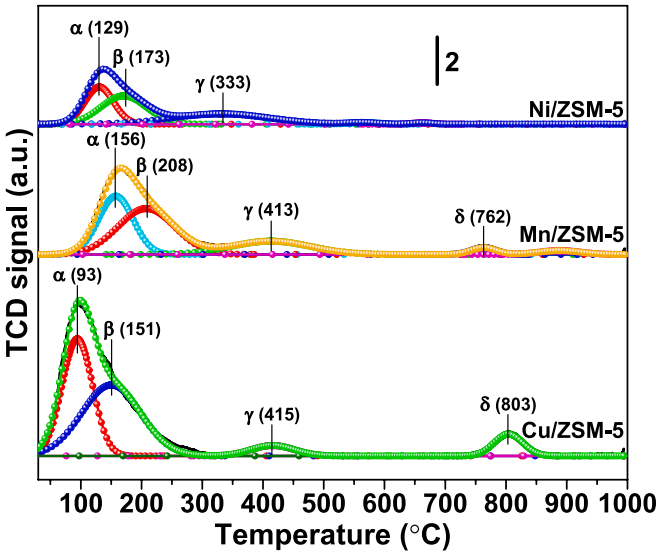

Fig. 6. O_2-TPD-TCD profiles of Cu/ZSM-5, Mn/ZSM-5 and Ni/ZSM-5 catalysts.

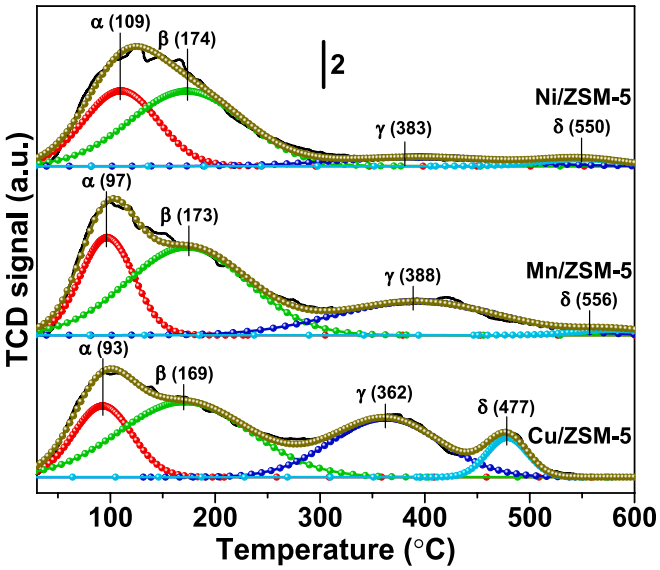

Fig. 7. NH_3-TPD-TCD profiles of Cu/ZSM-5, Mn/ZSM-5 and Ni/ZSM-5 catalysts.

to bind a significant amount of physisorbed NH_3 but also inhibit the adsorption of ammonia at Al–OH sites. The HT- peak > 450 °C (δ peak, strong acid sites) is assigned to coordinated ammonia bound to bulk copper and nickel oxides (Lewis acid sites, 476 °C for Cu/ZSM-5, and 535 °C for Ni/ZSM-5). Correspondingly, the signal monitored by a mass spectrometer (mass 28) provide evidence that the NH_3 adsorbed on Brønsted and Lewis acid sites is thermally desorbed to yield N_2 release. This finding is not surprising because the NH_3 adsorbed here is seen to extract the surrounding oxygen of metal oxides to complete this

Table 1
H_2 and O_2 uptake of catalysts.

Catalysts	H_2 consumption (mmol/g)			O_2 consumption (mmol/g)					
	α	β	Total	α	β	α + β	γ	δ	Total
Cu/ZSM-5	1.38	0.11	1.49	0.47	0.55	1.02	0.06	0.08	1.17
Mn/ZSM-5	0.16	0	0.16	0.21	0.26	0.47	0.11	0.02	0.60
Ni/ZSM-5	2.63	0.51	3.14	0.12	0.14	0.26	0.11	0	0.36

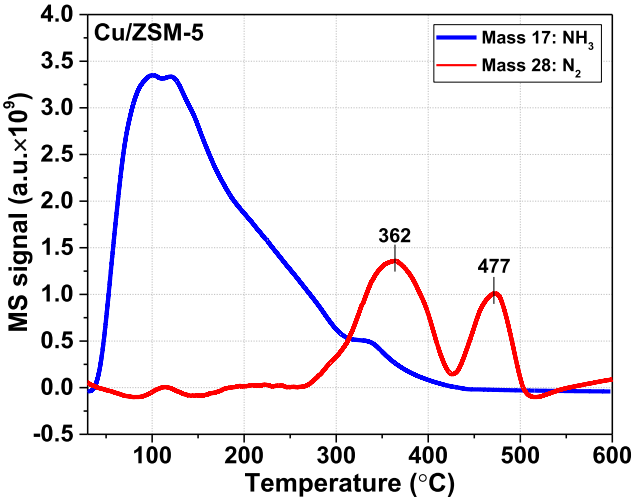

Fig. 8. NH_3-TPD-MS profiles of the Cu/ZSM-5 catalyst.

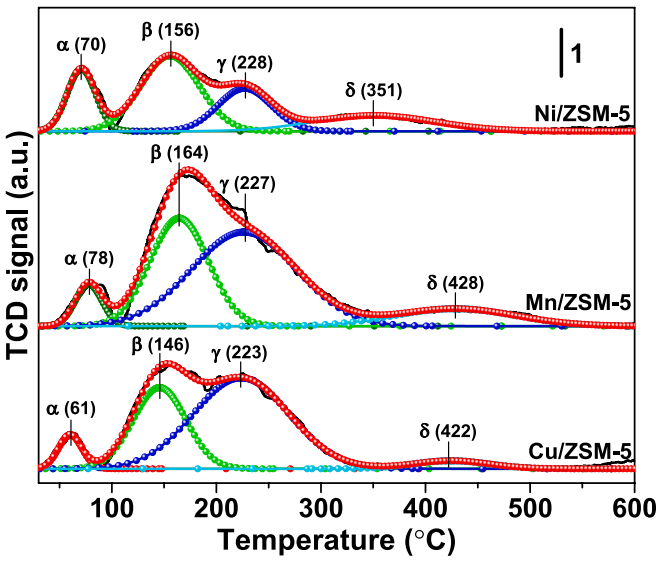

Fig. 9. NO-TPD-TCD profiles of Cu/ZSM-5, Mn/ZSM-5 and Ni/ZSM-5 catalysts.

oxidation, following the reduction of metal oxides. An impossible task is to quantify the desorption of NH_3 and N_2 by comparing MS peak areas because of the different mass spectrometer sensitivities for mass 17 and mass 28. As shown by the values quantified by peak areas of TCD (Table 2), Cu/ZSM-5 has the highest amount of medium acid sites with lowest strength, followed by Mn/ZSM-5 and then Ni/ZSM-5, indicating that the ammonia adsorbed on Cu/ZSM-5 is more easily activated and closely attributable to the low-temperature selective reduction of NO.

The dissociation of the adsorbed NO species is widely reported as the key step of SCR [47]. The desorption profiles of NO adsorbed on catalysts are shown in Fig. 9. As the temperature increases, the mass spectrometer is correspondingly coupled to monitor the signals of N_2 (mass 28), O_2 (mass 32), NO (mass 30), N_2O (mass 44), and NO_2 (mass 46), which are displayed in Fig. 10. All the catalysts exhibit two direct NO desorption peaks at 61–78 °C and 146–164 °C. The former (α peak) can be ascribed to physisorbed NO species on ZSM-5 support, and the latter (β peak) can be attributed to physisorbed NO species at metal sites with higher thermal stability. NO_2 is the recombination of NO cracking fragment (O atom) with NO in the mass spectrometer, which has been verified by a single NO injection test. Therefore, the low-temperature NO_2 peak can be deduced to arise from the synchronous signal of NO. In addition to NO desorption, the N_2O (mass 44) is also seen to desorb in two stages, where the peak centered in the range of 223–228 °C is attributed to the desorption of NO bounded to amorphous clusters and another peak at 351–428 °C corresponds to the adsorbed NO strongly bounded to bulk oxides. No evidence of N_2 (mass 28) and O_2 (mass 32) is apparent. NO is likely to be adsorbed on metal sites, and two N—O bonds are activated at elevated temperatures to convert into N_2O that desorbs into the gas phase, leaving an oxygen atom that leads to an increase in the metal valence. The peak heights and areas under NO and N_2O curves can therefore be compared directly with the data in Table 3. As for the more remarkable desorption band of N_2O (γ peak) at low temperature over Cu/ZSM-5, it supports the assumption that the relatively low bond strength between copper clusters and NO would facilitate the selective reduction of NO with NH_3 at low temperatures.

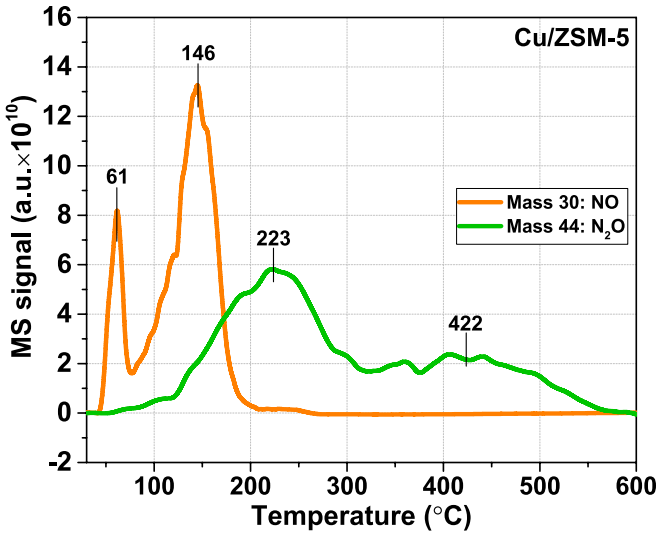

Fig. 10. NO-TPD-MS profiles of the Cu/ZSM-5 catalyst.

3.4. Catalytic performance

The catalytic performances of the Cu/ZSM-5, Mn/ZSM-5, and Ni/ZSM-5 catalysts for NH_3-SCR reaction is evaluated under the condition of 500 ppm NO + 500 ppm NH_3 + 5% O_2/N_2, with the results presented in Fig. 11. Ni/ZSM-5 shows relatively poor NH_3-SCR activity and two types of active sites including dispersed nickel clusters and bulk nickel oxides are formed on the Ni/ZSM-5 catalyst, resulting the abnormal activity by a two-step reaction process. The profile of NO can be described as a two-step reaction process, exhibiting an LT-peak at 290 °C with the NO conversion of 60.4% and an HT-peak at 460 °C with the NO

Table 2
NH_3-TPD quantitative results of catalysts.

Catalysts	NH_3 desorption (mmol/g)			N_2 formation (mmol/g)			Total NH_3 consumption (mmol/g)
	α	β	α + β	γ	δ	γ + δ	
Cu/ZSM-5	0.25	0.58	0.83	0.38	0.09	0.47	1.77
Mn/ZSM-5	0.30	0.62	0.92	0.31	0.02	0.34	1.59
Ni/ZSM-5	0.32	0.50	0.82	0.08	0.03	0.12	1.06

Table 3
NO-TPD quantitative results of catalysts.

Catalysts	NO desorption (mmol/g)			N_2O formation (mmol/g)			Total NO consumption (mmol/g)
	α	β	α + β	γ	δ	γ + δ	
Cu/ZSM-5	0.02	0.16	0.18	1.51	0.11	1.62	3.42
Mn/ZSM-5	0.03	0.19	0.23	1.88	0.40	2.28	4.78
Ni/ZSM-5	0.05	0.12	0.17	0.39	0.32	0.71	1.58

conversion of 90.9%. According to the SEM, NH_3-TPD and NO-TPD results mentioned above, nickel clusters dispersed on the ZSM-5 surface are the active phase for the SCR at LT-peak, where the NO adsorbed on the dispersed nickel sites reacts with NH_3 adsorbed on Brønsted acid sites to yield N_2 and H_2O. Excess nickel enriched to form bulk oxides are potentially a good candidate for performing SCR activity at the HT-peak, that is, the reaction taking place between NO and NH_3 adsorbed here. The two types of active sites are motivated in the temperature range of 150–290 and 420–460 °C, respectively. Therefore, the significant rate increase can be observed with temperature, where the overlap of the profiles of NO and NH_3 conversion implies that two reactants are consumed during SCR according to a chemical equivalence ratio of 1:1 ($4NO + 4NH_3 + O_2 \rightarrow 4\ N_2 + 6H_2O$). However, the conversion of NH_3 tends to be higher than that of NO after NO conversion passes through the maximum. This situation indicates that the role of the active sites—namely, amorphous and bulk nickel oxides—changes from promoting SCR to nonselective ammonia oxidation; the latter has also been confirmed by NH_3-TPD.

Cu/ZSM-5 and Mn/ZSM-5, especially the former, are more active than Ni/ZSM-5. The NO conversion for Cu/ZSM-5 can reach 90% at 221 °C, while Mn/ZSM-5 reached only 54.6% at the same reaction temperature. Moreover, the NO conversion for Mn/ZSM-5 reaches more than 90% in the temperature range of 276–427 °C, but Cu/ZSM-5 achieves more than 90% NO conversion at a broader operation temperature window (221–445 °C). The amorphous copper clusters enriched in the surface is responsible for the excellent SCR performance of Cu/ZSM-5, which has a relatively higher reducibility than that of Mn/ZSM-5 to promote the mass transfer of reactants or products during SCR. The reaction active energy of SCR (NO conversion < 20%) for Cu/ZSM-5, Mn/ZSM-5, and Ni/ZSM-5 is determined according to Arrhenius Eqs. (1) and (2)

$$k = A\exp\left(\frac{-E_r}{RT}\right) \tag{1}$$

$$\text{or}\ \ \ln k = \ln A - E_r/\mathrm{RT} \tag{2}$$

where k is the SCR rate, A is the pre-exponential factor, R is the gas constant, and T is the absolute temperature. With the use of the slope of the plot ln*(k)* versus 1000/T as plotted in Fig. 12, the activation energies (E_r) of SCR for these catalysts are calculated as 40.6 kJ/mol (Cu/ZSM-5), 45.1 kJ/mol (Mn/ZSM-5), and 57.2 kJ/mol (Ni/ZSM-5).

3.5. *In situ infrared spectroscopy*

The Cu/ZSM-5, Mn/ZSM-5, and Ni/ZSM-5 catalysts were pre-absorbed with 1.0 vol% NO + 10 vol%O_2/Ar (40 mL/min) for 30 min, then the 1.0 vol%NH_3 + 10 vol% O_2/Ar was introduced to react at 150 °C after purging with Ar (Fig. 13A, C, and E). The in situ IR spectra for each catalyst were detected in succession at 1-min intervals. The bands at 1898–1888 cm^{-1} are assigned to two kinds of –NO species; the bands at 1360 cm^{-1} are attributed to the hyponitrites and bridging monodentate nitrites ($N_2O_2^{2-}$), while the bands at 1629, 1598, and 1570 cm^{-1} belong to three kinds of nitrate species (—NO_2) [46]. When the $NH_3 + O_2$ is passed over the NO + O_2^- preadsorbed catalysts, the —NO and —NO_2 species disappear rapidly, indicating that these species are very active on the catalyst surface and can easily react with NH_3. However, the bands at 1294 and 1287 cm^{-1} assigned to the NH_3 species adsorbed on Lewis acid sites, while the 1738, 1522, and 1503 cm^{-1} related to NH_4^+ ions at Brønsted acid sites increased [48]. The reverse process was performed via preabsorption with 1.0 vol%NH_3 + 10 vol% O_2/Ar for 30 min, and 1.0 vol% NO + 10 vol%O_2/Ar was introduced to react at 150 °C, as shown in Fig. 13B, D, and F. The IR spectra clearly show that the NH_4^+ ions are at the Brønsted acid sites (1738 cm^{-1}) and the NH_3 species are adsorbed on the Lewis acid sites (1598 and 1287 cm^{-1}). After the NO + O_2 is introduced, the NH_4^+ ions and NH_3 species are consumed based on the decrease in peak intensity. This result indicates that both types of acid sites are involved in the SCR reaction.

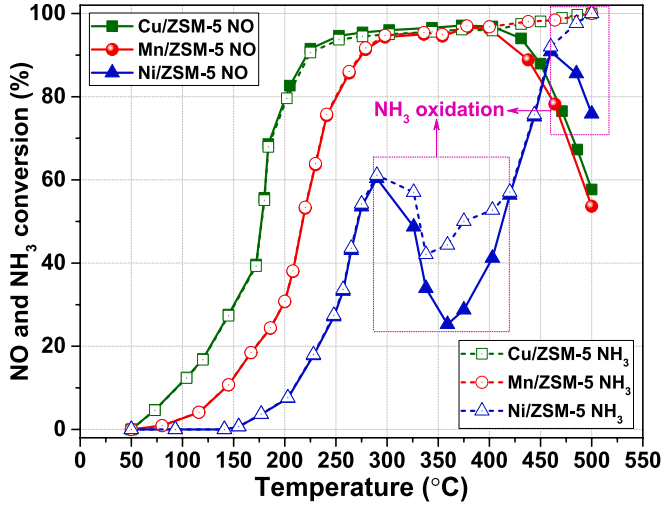

Fig. 11. SCR activity for NO and NH_3 conversion as a function of reaction temperature for Cu/ZSM-5, Mn/ZSM-5 and Ni/ZSM-5 catalysts.

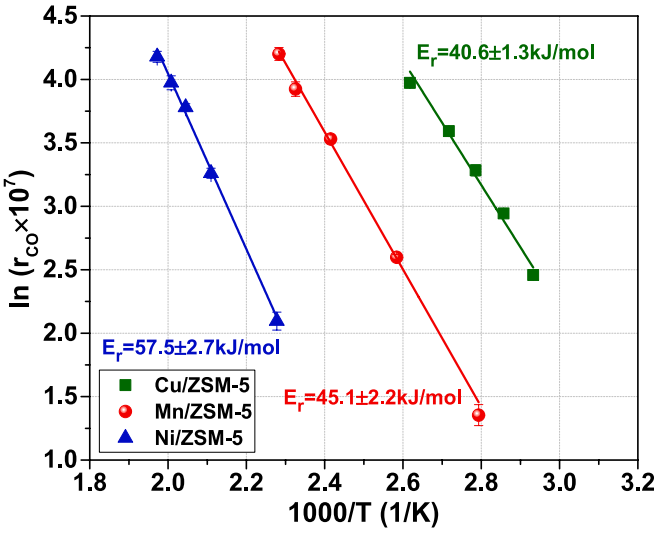

Fig. 12. Arrhenius plots of reaction rates determined according to the NO conversion during SCR reaction temperature lower than 15%.

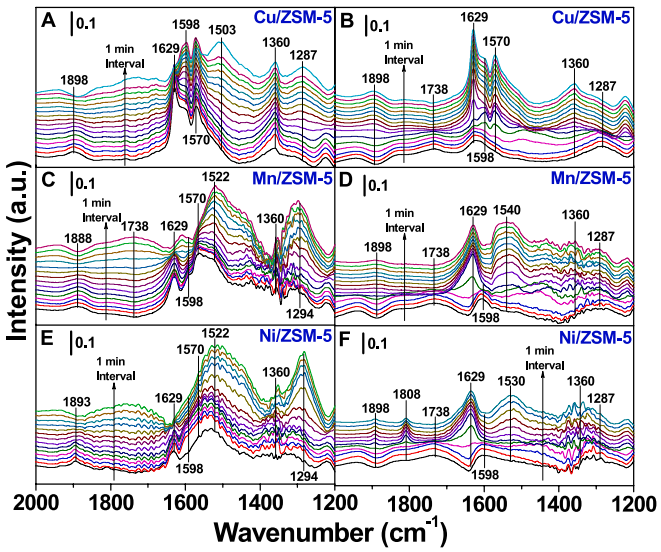

Fig. 13. In situ IR spectra of the reaction between NH_3 and pre-adsorbed NO + O_2 (A), (C) and (E), and between NO and pre-adsorbed NH_3 + O_2 (B), (D) and (F) on the catalysts at 150 °C for 15 min.

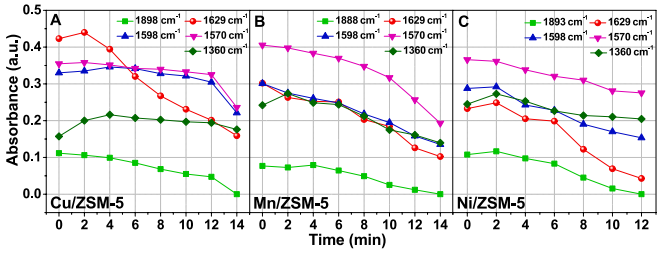

Fig. 14. Absorbance intensity variation of adsorbed NO_x species under the reaction between NH_3 and pre-adsorbed NO + O_2 at 150 °C.

Meanwhile, new bands are found in the three catalysts, which are attributed to the nitrate species (—NO_2), —NO species and hyponitrites, and bridging monodentate nitrites ($N_2O_2^{2-}$).

To reveal the contributions of different adsorbed NO_x species in the SCR reaction, the intensities for the —NO species (1898–1893 cm^{-1}), bridging nitrates (1629 cm^{-1}), chelating nitrates (1598 cm^{-1}), monodentate nitrates (1570 cm^{-1}), and free ionic nitrates (1360 cm^{-1}) of catalysts are obtained based on the data in Fig. 13A, C, and E, as shown in Fig. 14. All the intensities of peaks present a declining trend as the reaction time increases. The bridging nitrate intensity of Cu/ZSM-5 achieves the maximum initial absorbance values and reduces rapidly within 14 min, corresponding to 0.423 and 0.159. However, for Mn/ZSM-5 and Ni/ZSM-5, the bands associated with monodentate nitrates decay rapidly. A similar trend occurs for bridging nitrates, chelating nitrates, and monodentate nitrates, whereas the bands related to —NO species diminish slowly. Hence, the initial signal intensity and decreased rate of bridging nitrates species follow the order Cu/ZSM-5 > Mn/ZSM-5 > Ni/ZSM-5, which is in agreement with the order of activity results, thereby implying that the bridging nitrates act as a main contributor in the SCR reaction.

3.6. Mechanism of low-temperature SCR and determination of kinetic parameters

From the above results, the standard SCR process over metal-based ZSM-5 catalysts can be deduced to follow the L-H mechanism that the gaseous NO is absorbed on metal sites and further combines with the adjacent activated NH_3 species on Brønsted or Lewis acid sites to form N_2 and H_2O. According to the results of the activity test, the light-off temperature of SCR (defined as the temperature at 10% NO conversion, T_{10}) is 101, 142, and 212 °C for Cu/ZSM-5, Mn/ZSM-5, and Ni/ZSM-5, respectively. Hence, physically adsorbed species that desorbed at a temperature lower than T_{10} (NO—, NH_3— and O_2-TPD) can be estimated as not contributing to low-temperature SCR. Proposed reaction pathways are shown in Fig. 15. An already known fact is that the co-adsorption and interaction of NO and NH_3 on a high-valence metal site (M^{H+}, such as Cu^{2+}, Mn^{4+}, and Ni^{2+}) over the catalysts results in partial reduction to a low-valence metal site (M^{L+}, such as Cu^{+}, Mn^{2+}, and Ni^{0}) and the release of N_2 and H_2O as products. The process through which NO is reduced by NH_3 in the absence of O_2 is supported by the activity test, where the fact that adsorbed NO uptakes lattice oxygen of metals to form NO_2 can be excluded because no NO_2 signal can be detected during NO-TPD-MS analysis. The calculated adsorption energy of NO on Cu^{2+}-OH^- is −1.05 eV to yield a NO^+-Cu^+-OH species, which is quite close to the corresponding adsorption of NH_3, resulting in a NH_3-Cu^{2+}-OH species [26]. As this article discusses above, the adsorption heat (supplementary information) of NO and NH_3 (β peak) determined by NO- and NH_3-TPD is also similar. Thus, the actual order of adsorption of NO and NH_3 seems more or less random to reach equilibrium. Then, a proton is possibly generated on the adjacent Brønsted sites after reduction treatments, which interacts with adsorbed NH_3 species on Lewis sites, thereby yielding an intermediate NH_4^+ on Brønsted sites [49,50]. The Cu^{2+} cations clearly have the highest reducibility, followed by Mn^{4+} and then Ni^{2+}. Ni/ZSM-5 exhibits the lowest activity of SCR with higher nickel surficial enrichment than that of copper, while Mn/ZSM-5 with a tiny amount of MnO_2 as the active phase falls somewhere in the middle. Possibly, the high gas diffusivity $D_v \propto T^{1.81}$ and high mass transfer $K_s=(D_v \cdot S)^{1/2}$ (T denotes the temperature, and S denotes the turnover frequency) [51] of Mn/ZSM-5 favor the rise of the reaction rate with temperature. As highly mobile proton carriers, the formation of NH_4^+ intermediates is taken as the rate determining step of SCR at low temperatures, where the activity of Cu/ZSM-5, Mn/ZSM-5, and Ni/ZSM-5 can be linked with the desorption number and temperature of NH_3 on Brønsted sites, quantified from the NH_3 that evolved during TPD of NH_4-form species. Finally, the NH_4^+ intermediate reacts with NO and O_2 to desorb N_2 and H_2O, followed by a low-valence metal site that is reoxidized to a high-valence site. The NO reduced by NH_3 in absence of O_2 indicates that partially active lattice oxygen tends to participate more in the SCR process compared with adsorbed or gaseous O_2, and the created oxygen vacancies are immediately replenished by the dissociation of gaseous O_2 on the catalyst surface. As the bed temperature increases,

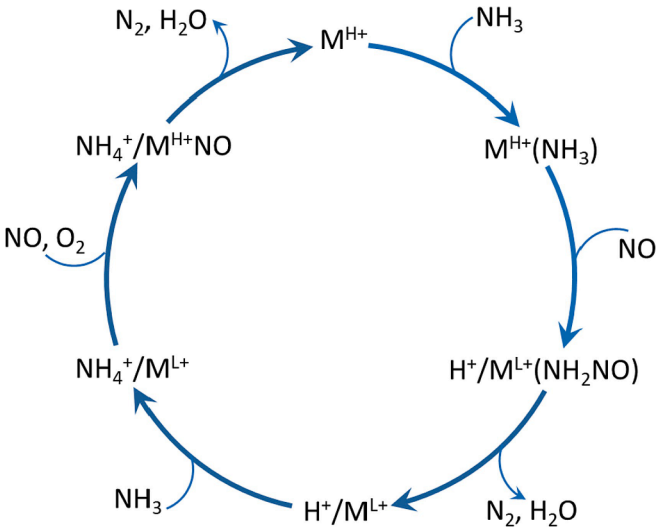

Fig. 15. proposed reaction pathways of SCR over the Cu/ZSM-5, Mn/ZSM-5 and Ni/ZSM-5 catalysts.

well-dispersed metal sites and bulk metal oxides participate in the SCR reaction in turn, and the latter follows a similar reaction mechanism as the former.

Considering the low-temperature activity of SCR induced by well-dispersed metal sites, the kinetic equations of NO and NH_3 conversion through the L-H mechanism can be described according to the reaction involving adsorbed NO and NH_3 molecules under a 500 ppm NO + 500 ppm NH_3 + 5% O_2/N_2 (P_{NO} = 50.5 Pa and P_{NH3} = 50.5 Pa) atmosphere. The following is a steady state at each reaction temperature among the rate of adsorption (R_a), desorption (R_d), and reaction (R_r) [52]:

$$R_a - R_d - R_r = 0 \tag{3}$$

For NO conversion,

$$k_{ano}P_{no}(1-\theta_{no}) - k_{dno}\theta_{no} - k_r\theta_{no}\theta_{nh} = 0 \tag{4}$$

For NH_3 conversion,

$$k_{anh}P_{nh}(1-\theta_{nh}) - k_{dnh}\theta_{nh} - k_r\theta_{no}\theta_{nh} = 0 \tag{5}$$

where θ_{no} and θ_{nh} denote the NO and NH_3 coverage arising from adsorbed NO and NH_3, respectively; P_{no}, P_{nh} are the partial pressures of NO and NH_3; k_{ano}, k_{anh}, k_{dno}, and k_{dnh} are the rate constants of adsorption and desorption of NO and NH_3; and k_r is the rate constant of low-temperature SCR. The exact solutions of Eqs. (4) and (5) are

$$\theta_{no} = \frac{K_{no}P_{no}}{1 + K_{no}P_{no} + (\frac{k_r}{k_{dno}})\theta_{nh}} \tag{6}$$

$$\theta_{nh} = \frac{K_{nh}P_{nh}}{1 + K_{nh}P_{nh} + (\frac{k_r}{k_{dnh}})\theta_{no}} \tag{7}$$

$K_{no} = k_{ano}/k_{dno}$ and $K_{nh} = k_{anh}/k_{dnh}$ are the adsorption coefficient of NO and NH_3, respectively. On the basis of the NO- and NH_3-TPD results, K_{no} and K_{nh} can be determined according to Langmuir's model [53] shown in the Supplementary Information, together with the corresponding adsorption heat of NO (E_{no}) and NH_3 (E_{nh}). The rate constant of low-temperature SCR (k_r) is given by Eq. (8)

$$k_r = \frac{kT}{h} \bullet \exp\left(\frac{-E_r}{RT}\right) \tag{8}$$

where h is the Planck's constant, and k is the Boltzmann's constant. The reaction active energy of E_{r1} is 40.6 kJ/mol (Cu/ZSM-5), 45.1 kJ/mol (Mn/ZSM-5), and 57.2 kJ/mol (Ni/ZSM-5) in Section 3.4. The k_{dno} and k_{dnh}, as rate constants of NO and NH_3 desorption, respectively, are determined by analogy with k_r, where active energies of NO and NH_3 adsorption can be ignored because NO and NH_3 adsorption is finished at room temperature. The theoretical reaction rate (R_r) is obtained numerically according to Eq. (9)

$$R_r = k_r\theta_{no}\theta_{nh} \tag{9}$$

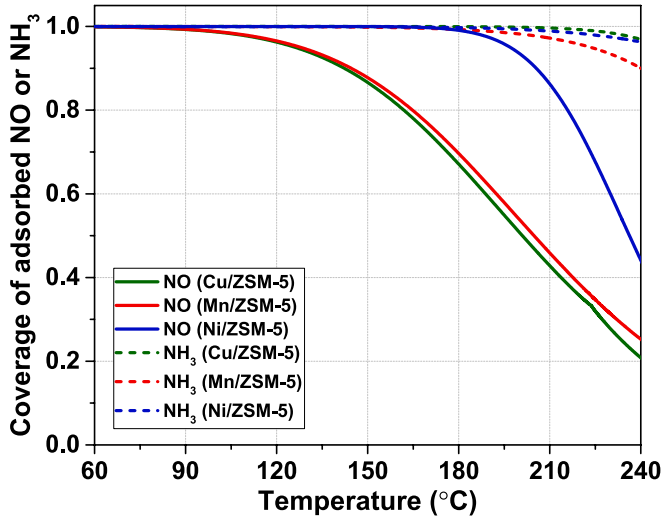

Fig. 16. Coverage of adsorbed NO and NH_3 over the Cu/ZSM-5, Mn/ZSM-5 and Ni/ZSM-5 catalysts.

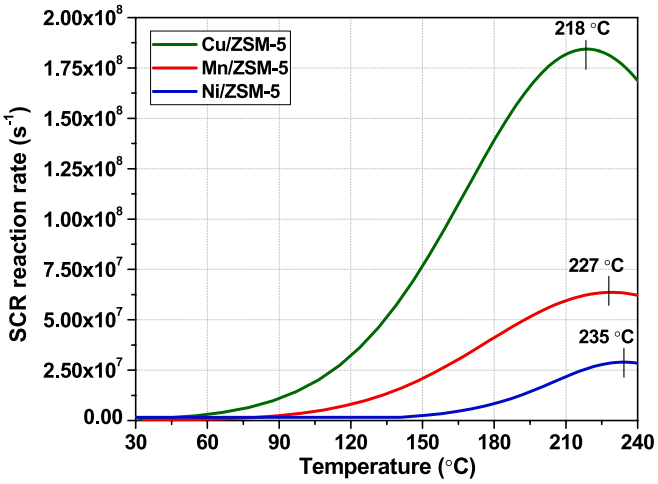

Fig. 17. SCR reaction rate over the Cu/ZSM-5, Mn/ZSM-5 and Ni/ZSM-5 catalysts.

The relevant kinetic parameters mentioned above are determined in the Supplementary Information, with the description of kinetic models, as illustrated in Figs. 16 and 17. The θ_{no} is more easily reduced with temperature than θ_{nh}, and the decay trends of θ_{no} and θ_{nh} over Cu/ZSM-5, Mn/ZSM-5, and Ni/ZSM-5 are in agreement with their adsorption curves and results of infrared spectroscopy. The SCR reaction rate represents related turnover frequency (s^{-1}) based on the coverage of adsorbed NO and NH_3 in this kinetic analysis. The SCR reaction rate of Cu/ZSM-5 is much higher than that of Mn/ZSM-5 and Ni/ZSM-5 because of their active energies of SCR, which enhances with temperature and reaches the maximum value of 1.8×10^8, 6.4×10^7, and 3.9×10^7 s^{-1} at 218, 227, and 235 °C, respectively. With the further increase in the temperature, the mass transfer limitation leads to the abrupt decrease in θ_{no} and reaction rate on the dispersed metal sites; therefore, the rate expression predicts volcano-type kinetic curves [54]. Such a phenomenon can be observed experimentally for Ni/ZSM-5 but not for Cu/ZSM-5 and Mn/ZSM-5. As the SCR rate falls, the NH_3 oxidation to N_2 prevails, where the adjacent NO that is adsorbed tends to react each other rather than with adsorbed NH_3 to yield N_2O. The dispersed and bulk copper/manganese sites possibly become active in the near-temperature range in turn, and those SCR profiles overlap with each other. Hence, Cu/ZSM-5 and Mn/ZSM-5 obtain broader temperature windows than Ni/ZSM-5 does.

4. Conclusions

In this paper, the NH_3-SCR performances for NOx reduction of transition metal (Cu, Mn, and Ni) supported ZSM-5 catalysts are investigated. Cu/ZSM-5 exhibited superior performances over the other two catalysts. To be specific, NO conversion of about 90% or above is obtained in the temperature range of 221–445 °C for Cu/ZSM-5, while this conversion was achieved at 276–427 °C for Mn/ZSM-5. Ni/ZSM-5 shows two peaks in the NO_x conversion profiles, which indicates that double active sites contribute to the activity of SCR reaction in turn with the increase in temperature. According to the SEM, XRD, and TEM results, copper and manganese can disperse well on the catalyst surface but nickel tends to form bulk NiO with a large crystallite size. The double active sites—namely, the dispersed metal oxide clusters and bulk metal oxides—are verified by H_2-TPR analysis, with the redox ability

following the order Cu/ZSM-5 > Mn/ZSM-5 > Ni/ZSM-5. The N_2O desorbs in two stages during NO-TPD, which is attributed to the desorption of NO bounded to amorphous clusters and the NO strongly bounded to bulk oxides. Evidently, two N—O bonds are activated to convert into N_2O release, leaving an oxygen atom that leads to the increase in the metal valence. Moreover, NH_3-TPD analysis testifies that the NH_3 adsorbed on both Brønsted and Lewis acid sites is thermally desorbed to yield N_2 release, where the adsorbed NH_3 extracts the lattice oxygen to complete this oxidation following the reduction of metal oxides. The double active sites, which may also contribute to SCR with NH_3, appear to cause nonselective oxidation of the reductant at higher temperatures. On the basis of the XPS results and in situ infrared spectroscopy, proposed reaction pathways can be established. The NO is first reduced by NH_3 in the absence of O_2 on a high-valence metal site. Accompanied by the reduction of the metal site, a lifted proton interacts with adsorbed NH_3 species on Lewis sites to yield an intermediate NH_4^+ on Brønsted sites. Then, the NH_4^+ intermediate reacts with NO and O_2 to desorb N_2 and H_2O, followed by the low-valence metal site reoxidized to the high-valence site. Finally, the kinetic equations of NO and NH_3 conversion through the L-H mechanism are described according to the reaction involving adsorbed NO and NH_3 molecules (both NO and NH_3 coverage). The SCR reaction rate of Cu/ZSM-5, Mn/ZSM-5, and Ni/ZSM-5 enhances with temperature and reaches the maximum value of 1.8×10^8, 6.4×10^7, and 3.9×10^7 s^{-1} at 218, 227, and 235 °C.

CRediT authorship contribution statement

Cheng Liu: Formal analysis, Investigation, Writing – original draft. **Running Kang:** Formal analysis, Investigation. **Feng Bin:** Funding acquisition, Writing – review & editing. **Xiaolin Wei:** Supervision, Resources, Project administration. **Kwun Nam Hui:** Methodology. **Saravanan Kasipandi:** Formal analysis. **Kwan San Hui:** Methodology, Writing – review & editing.

Declaration of Competing Interest

The authors declare that they have no known competing financial interests or personal relationships that could have appeared to influence the work reported in this paper.

Acknowledgments

This work is accomplished under the support of National Nature Science Foundation of China (No. 51736010), China Scholarship Council (No.202004910623). We sincerely thank Prof. Lv Gang (Tianjin University) for the reasonable suggestions about SCR reaction mechanism, and the Key Projects of Tianjin Natural Science Foundation (19JCZDJC40100).

Appendix A. Supplementary material

Supplementary data to this article can be found online at https://doi.org/10.1016/j.crcon.2021.11.002.

References

[1] S.Q. Ni, X.L. Tang, H.H. Yi, F.Y. Gao, C.Z. Wang, Y.R. Shi, R.C. Zhang, W.J. Zhu, Novel Mn-Ce bi-oxides loaded on 3D monolithic nickel foam for low-temperature NH3-SCR de-NOx: preparation optimization and reaction mechanism, J. Rare Earths. 2020.12.015. (Journal Pre-proof).
[2] D. Jo, T. Ryu, G.T. Park, P.S. Kim, C.H. Kim, I.-S. Nam, S.B. Hong, Synthesis of high-silica LTA and UFI zeolites and NH_3–SCR performance of their copper-exchanged form, ACS Catal. 6 (4) (2016) 2443–2447.
[3] R. Yua, Z.C. Zhaoa, S.J. Huangb, W.P. Zhang, Cu-SSZ-13 zeolite–metal oxide hybrid catalysts with enhanced SO2-tolerance in the NH3-SCR of NOx, Appl. Catal. B-Environ. 269 (2020), 118825.
[4] W. Zheng, J.-L. Chen, L. Guo, W.-B. Zhang, H.-R. Zhao, X.-Q. Wu, Research progress of hydrothermal stability of metal-based zeolite catalysts in NH3-SCR reaction, J. Fuel Chem. Technol. 48 (10) (2020) 1193–1210.
[5] J. Zhu, Z.D. Liu, L. Xu, T. Ohnishi, Y. Yanaba, M. Ogura, T. Wakihara, T. Okubo, Understanding the high hydrothermal stability and NH3-SCR activity of the fast-synthesized ERI zeolite, J. Catal. 391 (2020) 346–356.
[6] C.B. Jones, I. Khurana, S.H. Krishna, A.J. Shih, W.N. Delgass, J.T. Miller, F. H. Ribeiro, W.F. Schneider, R. Gounder, Effects of dioxygen pressure on rates of NO_x selective catalytic reduction with NH_3 on Cu-CHA zeolites, J. Catal. 389 (2020) 140–149.
[7] J.B. Lim, J. Shin, N.H. Ahn, I. Heo, S.B. Hong, Selective catalytic reduction of NO with CH_4 over cobalt-exchanged cage-based, small-pore zeolites with different framework structures, Appl. Catal. B-Environ. 267 (2020), 118710.
[8] H.I. Hamoud, V. Valtchev, M. Daturi, Selective catalytic reduction of NO_x over Cu- and Fe-exchanged zeolites and their mechanical mixture, Appl. Catal. B-Environ. 250 (2019) 419–428.
[9] T.T. Le, A. Chawla, J.D. Rimer, Impact of acid site speciation and spatial gradients on zeolite catalysis, J. Catal. 391 (2020) 56–68.
[10] J. Dědeček, E. Tabor, S. Sklenak, Tuning the aluminum distribution in zeolites to increase their performance in acid-catalyzed reactions, Chemsuschem. 12 (3) (2019) 556–576.
[11] B.C. Knott, C.T. Nimlos, D.J. Robichaud, M.R. Nimlos, S. Kim, R. Gounder, Consideraton of the aluminum distribution in zeolites in theoretical and experimental catalysis research, ACS Catal. 8 (2018) 770–784.
[12] H.A. Habib, R. Basner, R. Brandenburg, U. Armbruster, A. Martin, Selective catalytic reduction of NO_x of ship diesel engine exhaust gas with C_3H_6 over Cu/Y zeolite, ACS Catal. 4 (8) (2014) 2479–2491.
[13] U. Deka, I. Lezcano-Gonzalez, B.M. Weckhuysen, A.M. Beale, Local environment and nature of Cu active sites in zeolite-based catalysts for the selective catalytic reduction of NO_x, ACS Catal. 3 (3) (2013) 413–427.
[14] Y. Mao, Z. Wang, H.F. Wang, P. Hu, Understanding catalytic reactions over zeolites: a density functional theory study of selective catalytic reduction of NO_x by NH_3 over Cu-SAPO-34, ACS Catal. 6 (2016) 7882–7891.
[15] C. Chupin, A. Vanveen, M. Konduru, J. Despres, C. Mirodatos, Identity and location of active species for NO reduction by CH_4 over Co-ZSM-5, J. Catal. 241 (1) (2006) 103–114.
[16] T. Selleri, I. Nova, E. Tronconi, The low-temperature interaction of NH_3/NO/NO_2+O_2 with Fe-ZSM-5+BaO/Al_2O_3 and H-ZSM-5+BaO/Al_2O_3: Influence of phase separation and relevance for the NH_3-SCR chemistry, Appl. Catal. B-Environ. 206 (2017) 471–478.
[17] A. Bellmann, H. Atia, U. Bentrup, A. Brückner, Mechanism of the selective reduction of NO_x by methane over Co-ZSM-5, Appl. Catal. B-Environ. 230 (2018) 184–193.
[18] M. Mizumoto, N. Yamazoe, T. Seiyama, Catalytic reduction of NO with ammonia over Cu(II) NaY, J. Catal. 55 (1978) 119–128.
[19] J.A. Sullivan, O. Keane, The role of Bronstead acidity in poisoning the SCR-urea reaction over FeZSM-5 catalysts, Appl. Catal. B-Environ. 61 (3-4) (2005) 244–252.
[20] S. Kieger, G. Delahay, B. Coq, B. Neveu, Selective catalytic reduction of nitric oxide by ammonia over Cu-FAU catalysts in oxygen-rich atmosphere, J. Catal. 183 (2) (1999) 267–280.
[21] T.S. Li, S.H. Li, J.T. Li, H.Z. Li, X.X. Wu, Efficient and convenient procedures for the formation and cleavage of steroid acetals catalysed by montmorilloaite, Chinese Chem. Lett. 7 (1996) 975–978.
[22] F. Bin, C. Song, G. Lv, J. Song, X. Cao, H. Pang, K. Wang, Structural characterization and selective catalytic reduction of nitrogen oxides with ammonia: a comparison between Co/ZSM-5 and Co/SBA-15, J. Phys. Chem. C 116 (2012) 26262–26274.
[23] M. Fu, C. Li, P. Lu, L. Qu, M. Zhang, Y. Zhou, M. Yu, Y. Fang, A review on selective catalytic reduction of NO_x by supported catalysts at 100–300 °C-catalysts, mechanism, kinetics, Catal. Sci. Technol. 4 (1) (2014) 14–25.
[24] V. Rizzotto, D. Chen, B.M. Tabak, Ji Yang, D. Ye, U. Simon, P. Chen, Spectroscopic identification and catalytic relevance of NH4+ intermediates in selective NOx reduction over Cu-SSZ-13 zeolites, Chemosphere 250 (2020), 126272.
[25] H. Wang, Z. Qu, S. Dong, C. Tang, Mechanism study of FeW mixed oxides to the selective catalytic reduction of NO_x with NH_3: in situ DRIFTS and MS, Catal. Today 307 (2018) 35–40.
[26] T.V.W. Janssens, H. Falsig, L.F. Lundegaard, et al., A consistent reaction scheme for the selective catalytic reduction of nitrogen oxides with ammonia, ACS Catal. 5 (2015) 2832–2845.
[27] Y.J. Pan, B.X. Shen, L.J. Liu, Y. Yao, H.P. Gao, C. Liang, H.J. Xu, Develop high efficient of NH_3-SCR catalysts with wide temperature range by ball-milled method, Fuel 282 (2020), 118834.
[28] W.S. Kijlstra, D.S. Brands, E.K. Poels, A. Bliek, Mechanism of the selective catalytic reduction of NO by NH_3 over MnO_x/Al_2O_3, J. Catal. 171 (1) (1997) 208–218.
[29] M. Stanciulescu, P. Bulsink, G. Caravaggio, L. Nossova, R. Burich, NH_3-TPD-MS study of Ce effect on the surface of Mn- or Fe-exchanged zeolites for selective catalytic reduction of NO_x by ammonia, Appl. Surf. Sci. 300 (2014) 201–207.
[30] O.A. Zelekew, D.-H. Kuo, Facile synthesis of SiO_2@Cu_xO@TiO_2 heterostructures for catalytic reductions of 4-nitrophenol and 2-nitroaniline organic pollutants, Appl. Surf. Sci. 393 (2017) 110–118.
[31] M. Thommes, K. Kaneko, A.V. Neimark, J.P. Olivier, F. Rodriguez-Reinoso, J. Rouquerol, K.S.W. Sing, Physisorption of gases with special reference to the evaluation of surface area and pore size distribution, Pure Appl. Chem. 87 (2015) 1051–1069.
[32] M.C. Biesinger, L.W.M. Lau, A.R. Gerson, R.S.C. Smart, Resolving surface chemical states in XPS analysis of first row transition metals, oxides and hydroxides: Sc, Ti, V, Cu and Zn, Appl. Surf. Sci. 257 (3) (2010) 887–898.
[33] N.S. McIntyre, S. Sunder, D.W. Shoesmith, F.W. Stanchell, J. Vac. Sci. Technol. 18 (1981) 714.

[34] P. Gaudin, P. Fioux, S. Dorge, H. Nouali, M. Vierling, E. Fiani, M. Molière, J.-F. Brilhac, J. Patarin, Formation and role of Cu^{+} species on highly dispersed CuO/SBA-15 mesoporous materials for SO_x removal: An XPS study, Fuel Process. Technol. 153 (2016) 129–136.
[35] J. Jiang, A. Kucernak, Electrochemical supercapacitor material based on manganese oxide: preparation and characterization, Electrochim. Acta 47 (2002) 2381–2386.
[36] M.C. Biesinger, B.P. Payne, A.P. Grosvenor, L.W.M. Lau, A.R. Gerson, R.St. C. Smart, Resolving surface chemical states in XPS analysis of first row transition metals, oxides and hydroxides: Cr, Mn, Fe, Co and Ni, Appl. Surf. Sci. 257 (2011) 2717–2730.
[37] G. Pantaleo, V. La Parola, F. Deganello, R.K. Singha, R. Bal, A.M. Venezia, Ni/CeO_2 catalysts for methane partial oxidation: Synthesis driven structural and catalytic effects, Appl. Catal. B-Environ. 189 (2016) 233–241.
[38] M.C. Biesinger, B.P. Payne, L.W.M. Lau, A. Gerson, R. St, C. Smart, X-ray photoelectron spectroscopic chemical state quantification of mixed nickel metal, oxide and hydroxide systems, Surf. Interface Anal. 41 (2009) 324–332.
[39] Y. Shu, M. He, J. Ji, H. Huang, S. Liu, D.Y.C. Leung, Synergetic degradation of VOCs by vacuum ultraviolet photolysis and catalytic ozonation over Mn-xCe/ZSM-5, J. Hazard. Mater. 364 (2019) 770–779.
[40] R.W. Millar, Specific heats of manganese oxides, J. Amer. Chem. Soc. 50 (1928) 1875–1883.
[41] J.C. Southard, C.H. Shomate, Heat of formation and high-temperature heat content of manganous oxide and manganous sulfate. High-temperature heat content of manganese, J. Amer. Chem. Soc. 64 (1942) 1770–1774.
[42] A.M. Rabie, M.A. Betiha, S.-E. Park, Direct synthesis of acetic acid by simultaneous co-activation of methane and CO_2 over Cu-exchanged ZSM-5 catalysts, Appl. Catal. B-Environ. 215 (2017) 50–59.
[43] E.V. Rebrov, A.V. Simakov, N.N. Sazonova, V.A. Rogov, G.B. Barannik, Propane and oxygen action on NO_x adspecies on low-exchanged Cu-ZSM-5, Catal. Lett. 51 (1998) 27–40.
[44] L. Zhu, J. Yu, X. Wang, Oxidation treatment of diesel soot particulate on $Ce_xZr_{1-x}O_2$, J. Hazard. Mater. 140 (1-2) (2007) 205–210.
[45] F. Bin, C. Song, G. Lv, J. Song, X. Cao, H. Pang, K. Wang, Structural characterization and selective catalytic reduction of nitrogen oxides with ammonia: a comparison between Co/ZSM–5 and Co/SBA-15, J. Phys. Chem. C 116 (2012) 26262–26274.
[46] F. Bin, C. Song, G. Lv, J. Song, S. Wu, X. Li, Selective catalytic reduction of nitric oxide with ammonia over zirconium-doped copper/ZSM-5 catalysts, Appl. Catal. B-Environ. 150-151 (2014) 532–543.
[47] L. Zhong, W. Cai, Y. Yu, Q. Zhong, Insights into synergistic effect of chromium oxides and ceria supported on Ti-PILC for NO oxidation and their surface species study, Appl. Surf. Sci. 325 (2015) 52–63.
[48] T. Gu, R. Jin, Y. Liu, H. Liu, X. Weng, Z. Wu, Promoting effect of calcium doping on the performances of MnO_x/TiO_2 catalysts for NO reduction with NH3 at low temperature, Appl. Catal. B-Environ. 129 (2013) 30–38.
[49] P. Chen, M. Jabłońska, P. Weide, T. Caumanns, T. Weirich, M. Muhler, R. Moos, R. Palkovits, U. Simon, Formation and effect of NH^{4+} intermediates in NH_3-SCR over Fe-ZSM–5 zeolite catalysts, ACS Catal. 6 (11) (2016) 7696–7700.
[50] P. Chen, R. Moos, U. Simon, Metal loading affects the proton transport properties and the reaction monitoring performance of Fe-ZSM-5 and Cu-ZSM–5 in NH_3–SCR, J. Phys. Chem. C 120 (44) (2016) 25361–25370.
[51] W.L. Mccabe, J.C. Smith, Peter Harriott, Scilab code for unit operations of chemical engineering, Chem. Eng. Unit Oper. 4 (1993) 527–565.
[52] A. Bourane, D. Bianchi, Oxidation of CO on a Pt/Al_2O_3 catalyst: from the surface elementary steps to light-off tests V. Experimental and kinetic model for light-off tests in excess of O_2, J. Catal. 222 (2004) 499–510.
[53] J. Nordstrand, J. Dutta, Dynamic langmuir model: a simpler approach to modeling capacitive deionization, J. Phys. Chem. C 123 (2019) 16479–16485.
[54] G. Avgouropoulos, T. Ioannides, Kinetics of CO and H_2 oxidation over $CuO\text{-}CeO_2$ and CuO catalysts, Chem. Eng. J. 176–177 (2011) 14–21.